Finite element global buckling analysis of tapered curved laminates

S. Akhlaque-E-Rasul[1] and R. Ganesan

Concordia Center for Composites, Department of Mechanical and Industrial Engineering, Concordia University, 1455 De Maisonneuve W., Montreal, QC, Canada, H3G 1M8.

[1]E-mail: akhlaque1045@hotmail.com

Abstract

Due to the variety of configurations of tapered curved composite plates the analysis becomes complex. At present no existing work deals with their response to compressive loading except the other works of present authors. The linear and non-linear buckling analyses of tapered curved composite plates are conducted in the present work using SHELL99 element of ANSYS®. The results obtained using ANSYS® are compared with that of the Finite Element Analysis using a Lagrange element based on First order Shell Theory (FST), and Ritz solution based on Classical Shell Theory (CST) and FST. The strength characteristics and load carrying ability of the tapered curved plates are investigated considering first-ply failure and delamination failure. Based on these analyses, the critical sizes and parameters of the tapered curved plates that will not fail before global buckling are determined. A parametric study is also carried out.

Key words: *Tapered curved plates, Buckling, Failure analyses*

1. Introduction

Piskunov and Sipetov (1987) have proposed a laminated tapered shell structure which accounts the effects produced by transverse shearing strain. They have developed a shearing strain model to minimize the differences between the physicomechanical parameters (the values of the elasticity modulus, the shear modulus, the Poisson ratio, the thermal conductivity coefficient, the linear expansion coefficient, etc.) of the composite layers. Another work on tapered laminated shell structure was conducted by Kee and Kim (2004), where the rotating blade is assumed to be a moderately thick, width-tapered in longitudinal direction and open cylindrical shell that includes the transverse shear deformation and rotary inertia, and is oriented arbitrarily with respect to the axis of rotation to consider the effects of disc radius and setting angle. The finite element method is used for solving the governing equations. Tennyson (1975) has conducted a brief review on static buckling theory for both geometrically perfect and imperfect anisotropic composite circular thin cylinders for various loading configurations. A review work on the problem of buckling of uniform-thickness and moderately-thick, laminated, composite shells subjected to destabilizing loads has been carried out by Simitses (1996). The World-Wide Failure Exercise (WWFE) contained a detailed assessment (Soden et al, 2004) of 19 theoretical approaches for predicting the deformation and failure response of polymer composite laminates when subjected to complex states of stress. The leading five theories (Zinoviev, Bogetti, Puck, Cuntze and Tsai) are explored in greater detail to demonstrate their strengths and weaknesses in predicting various types of structural failure. According to the investigations of

WWFE, Tsai-Wu theory is the best one that can be used to predict the first-ply failure of unidirectional laminates and any of the above mentioned five failure theories can be used for multidirectional laminates. Kant and Swaminathan (2000) have reviewed the different methods used for the estimation of transverse/interlaminar stresses in laminated composite plates and shells. Both analytical and numerical methods are considered. Salamon (1980) has presented a review and assessment of the interlaminar delamination problem common to layered composite materials. The work covers calculation of interlaminar stresses from a homogeneous and microstructural material viewpoint. The observation of edge delamination and experimental efforts are discussed together with the fracture mechanics studies. Bolotin (2001) has surveyed the literature and the mechanical aspects of delaminations in laminate composite structures. He discussed the surface and internal delaminations of various origin, shape and location. He also analyzed the origination, stability, and post-critical behavior of delaminations under quasi-static, cyclic, and dynamic loads.

Fig. 1

In the present work, the buckling response of tapered curved composite plates with longitudinal-internal-ply-drop-off configurations as shown in Fig. 1 is investigated. In the Fig. 1, h_{tk} and h_{tn} are the thicknesses at the thick end and the thin end respectively; L_{tk}, L_{tap} and L_{tn} are the lengths of thick, taper and thin section respectively; R, b and b' are the radius, the width and the cord length of a curved plate respectively; and (u_o, v_o, w_o) is the mid-plane displacement field that is referred to the global coordinate system (x, y, z). The taper configuration has five resin pockets: four small resin pockets are distributed symmetrically with respect to mid-plane and the fifth one is designed combining the two small resin pockets. Every small resin pocket is formed by dropping off three composite plies and there are continuous composite plies above and below these resin pockets. The Hybrid configuration is modeled combining the tapered and uniform-thickness sections as shown in the Fig. 1 wherein L denotes the total length of the hybrid plate.

2. Modeling

To model the tapered curved plates, the work-plane of ANSYS® was set perpendicular to x-axis and several curved lines (arcs) were drawn parallel to the yz plan by using the center and radius options. The curved lines are shown in the Fig. 2. Nine curved areas were created to relate the nine real constants for the tapered cross-section. Fifteen curved areas were created for the hybrid (tapered and uniform) cross-section. Finally, the areas were glued.

Fig. 2

3. Meshing

Element SHELL99 is used for the analyses using ANSYS®. SHELL99 is an 8-node, 3-D shell element with six degrees of freedom (three translations and three rotations) at each node. It is designed based on the degenerated solid approach with shear deformation effect and to model thin to moderately-thick plate and shell structures with a side-to-thickness ratio of roughly 10 or greater. The tapered curved plates are meshed by using eighty-one elements which are shown by numbering in the Fig. 2. Different real constants were assigned corresponding to the longitudinal

cross-sections of the laminates. The material properties of composite ply and epoxy resin are given in the Tables 1 and 2 respectively where X^t, Y^t and Z^t are the normal tensile strengths in the principal material directions $x"$, $y"$ *and* $z"$ respectively; R_{yz}, S_{xz} and T_{xy} are the shear strengths in the $y"z"$, $x"z"$ and $x"y"$ planes respectively; X^c, Y^c and Z^c are the normal compressive strengths in the principal material directions $x"$, $y"$ *and* $z"$ respectively. Based on the convergence test, the mesh selected and used for the taper configuration and hybrid configuration are 9×9 and 15×15 respectively.

Table 1
Table 2

4. Validation

The buckling analysis result obtained using ANSYS® is compared with that of the experimental and analytical solution. A uniform-thickness cylindrical panel made of T300/5208 graphite/epoxy having the mechanical properties of $E_{x"} = 141.34$ GPa (20.5×10^6 psi), $E_{y"} = 8.96$ GPa (1.3×10^6 psi), $G_{x"y"} = 5.17$ GPa (0.75×10^6 psi), $\upsilon_{x"y"} = 0.335$; clamped in transverse direction and simply supported in longitudinal direction are considered. The dimensions of the plate are taken to be: length L = 0.3048 m (12 inches), cord $b' = 0.3048$ m, radius R = 0.3048 m, the thickness $h = 1.016 \times 10^{-03}$ m (0.04 inches). Becker (1979) has conducted the bifurcation (obtained from eigenvalue solution) buckling analysis of this curved plate using STAGS computer code. The results are compared in the Table 3.

Table 3

As can be observed from the Table 3, the result obtained in the present work is higher than the theoretical and experimental buckling loads given in the reference works. According to Becker (1979), the bifurcation buckling load may be 23 to 45 percent higher than the experimental result for the critical buckling load. The difference between the boundary conditions imposed in the references and numerical solution using ANSYS® may also be a reason for the disagreement between the results.

5. Parametric study

5.1 First-ply failure analysis

The strength in compression of the tapered curved plate is investigated considering first-ply failure. This type of failure analysis is considered in the present work to determine whether any layer has failed (locally) due to compressive loading before the laminate as a whole fails on global buckling. First-ply failure analysis is carried out using ANSYS® based on the 3-D version of Tsai-Wu failure criterion given in the ANSYS® reference manual. The first-ply failure refers to the first instant at which any layer or more than one layer fails at the same load. The same criterion is applied for both the composite ply and the resin pocket. For this purpose, the resin pocket is considered (imagined) to be made up of layers of isotropic resin material. Material properties of composite ply and epoxy resin are given in the Tables 1 and 2 respectively.

Four square-shaped tapered composite plates of different sizes with the taper configuration (Fig. 1) and made of NCT/301 graphite-epoxy composite material are considered. The lay-up configuration for all the plates is $[0/90]_{9s}$ at the thick end and $[0/90]_{3s}$ at the thin end. This laminate is referred to as the laminate with lay-up configuration LC_1 in the Table 4 and further onwards. The side length of each of the square plates is as given in the Table 5, plate thickness at the thick end (h_{tk}) is 4.5 mm and the radius (R) of the plates is 500 mm. The clamped-clamped boundary conditions are considered. The results of first-ply failure analysis are summarized in the Table 5 along with the results of buckling analysis.

Table 4

In the Table 5, the first-ply failure loads are compared with the buckling loads. As can be seen from this table, the tapered curved plates corresponding to taper angles of 0.75 and 1.0 degrees will fail before the global buckling. On the other hand, the plates corresponding to taper angles of 0.1 and 0.50 degrees will not fail by first-ply failure loads at the state of global buckling. Therefore, the maximum plate size should be corresponding to a taper angle of 0.5 degree and the critical length-to-height ratio (L_{tap} / h_{tk}) is to be 36. The failed layers numbered 2 and 3 respectively are the second layer and the third layer from the bottom surface of the laminate at the thick end of the plate. All the tapered curved plates failed at the thick end where the numbers of plies above or below the resin pockets are at minimum.

Table 5

5.2 Delamination failure analysis

The initiation of delamination, if any, is dictated by the transverse interlaminar stresses developed under compressive load. In ANSYS®, interlaminar transverse shear stresses in shell element are calculated based on the assumption that no shear is carried at the top and bottom surfaces of the element. These interlaminar shear stresses are only computed in the interior of the element and are computed using equilibrium requirements. Delamination at any interface between any two adjacent layers is said to have occurred when any of the transverse stress components in any of the two layers adjacent to the interface becomes equal to or greater than its corresponding allowable strength. Four square tapered composite plates of different sizes with the taper configuration and made of NCT/301 graphite-epoxy composite material are considered. The lay-up is $[0/90]_{9s}$ at the thick end and $[0/90]_{3s}$ at the thin end which together is defined as lay-up configuration LC_1 in the Table 4. The material properties of the composite ply and epoxy material are given in the Tables 1 and 2 respectively. The side length of the square plate varies from 85.9 to 859.4 mm, plate thickness at the thick end (h_{tk}) is 4.5 mm and radius (R) of the plates is 500 mm. The clamped-clamped boundary conditions are considered. The averaged maximum interlaminer shear stresses are calculated in the present work at the state of first-ply failure load or critical buckling load (considering the larger one) and the corresponding locations are tabulated in the Table 6. The failed layers numbered 5 and 13 are, respectively, below and above the large resin pocket at the thin end.

It is observed from the Table 6 that no initiation of delamination takes place for the taper configuration and lay-up configuration LC_1 at the states of first-ply failure or global buckling. This is so because the maximum interlaminer shear stress in both the cases is less than the corresponding allowable shear strength of the composite material.

Table 6

As an alternative approach, thin resin layers of thickness 0.0125 mm each are considered above the top resin pockets and below the bottom resin pockets as shown by the thick lines (thick lines are used to show these layers more clearly) in the Fig. 3; these thin resin plies are defined as 'resin-rich layers'. The longitudinal cross-section across the middle of curved laminate is considered. The thin resin-rich layers having thickness of one-tenth of a composite ply are taken into account in the analysis and transverse interlaminar normal and shear stresses developed at the locations of the ply drop-off are calculated to determine the stress states at these locations. The plate with a taper angle of 1 degree corresponding to the data given in the Table 5 is investigated using the same boundary conditions, ply-configuration (LC_1) and material properties (Table 1 and Table 2). The stresses are calculated under the compressive load of 92.08×10^4 N/m which is the critical buckling load corresponding to taper angle of 1 degree. The stresses at the top thin 'resin-rich layers' in the global coordinate directions (x,y,z) are plotted in the Fig. 4.

Fig. 3
Fig. 4

From the stress distributions in 'resin-rich layers' shown in the Fig. 4, it is observed that significant normal and transverse stresses are present at these locations. These stresses are localized close to the region near the ply drops which are the probable locations for the initiation of delamination. In the Table 6, only the locations of maximum interlaminer stresses are identified but the present alternate approach is required to observe the distribution of these stresses along longitudinal direction. The drop in the normal stress σ_{zz} at each ply drop-off location is relatively higher than that in the interlaminar shear stresses. In addition, the drop in σ_{zz} at the ply drop-off that is close to the thin end is relatively the largest. A similar stress distribution has been observed at the bottom thin resin-rich layers.

5.3 Critical size of the tapered curved plate

The tapered plates of the Table 5 are analyzed corresponding to different radii using the clamped-clamped boundary conditions, taper configuration, and the material properties of Tables 1 and 2. The critical sizes of the tapered curved plates are determined corresponding to various radii. For the calculation of critical length-to-height ratio, the same procedure is applied as that used in the previous case of the plate with the radius of 500 mm. In the Fig. 5, the plot of radius versus critical length-to-height ratio of tapered curved plates is given. In this figure, L_{tap} denotes the taper length and h_{tk} denotes the thickness of the plate at the thick end. From Fig. 5, the following observations are made:

a) The critical length-to-height ratio of the plate increases with the decrease of radius. This is so because the stiffness of the tapered curved plate increases with the decrease of radius. The critical length-to-height ratio varies non-linearly with the radius. In the case of larger radius, shorter plate can be used under uni-axial compression, which will not fail before global buckling.
b) The design limit for the tapered curved composite plates mentioned in the Table 5 corresponds to the shaded area of the Fig. 5. Beyond this limit, tapered curved plate will fail by ply failure before global buckling of the plate occurs. Dark shaded area represents

the design limit predicted by the non-linear buckling analysis, and the dark and light shaded areas together represent the design limit corresponding to the linear buckling analysis.

Fig. 5

5.4 Behavior of Hybrid Curved Plates

The hybrid configuration (with tapered and uniform-thickness sections) is taken into account in the present section. The tapered section of hybrid plate is modeled using the taper configuration shown in Fig. 1 and three types of lay-up configurations, namely LC_1, LC_2 and LC_3 given in the Table 4 are considered. For the buckling analysis, a width of b = 114.6 mm and the material properties given in Tables 1 and 2 are considered. Figs. 6-8 show the variation of linear critical buckling load with the increase of radius calculated using different solution methods.

Fig. 6
Fig. 7
Fig. 8

From Figs. 6-8, the following observations are made.

a) The critical buckling loads of all lay-up configurations decrease with the increase of radius-to-thickness ratio.
b) The lowest and highest values of critical buckling loads are obtained using the FST-based Ritz solution and CST-based Ritz solution respectively. In the case of classical shell theory (CST), shear strains are omitted which is the cause for the corresponding higher values of buckling loads compared to that of the other three solutions. The critical buckling load calculated using FEM is lower than that of the ANSYS®. Because FEM solution is based on a 9-node shell element which has more degrees of freedom than that of the SHELL99 of ANSYS®.

6. Conclusions

The critical buckling loads calculated using ANSYS® are higher than that obtained using FEM and FST-based Ritz solution. The critical size and the critical buckling load of tapered/hybrid curved plates decease with the increase of radii. At higher value of radius, lay-up configurations LC_3, LC_1 and LC_2 become the strongest, moderate and weakest laminate respectively.

Acknowledgement

The authors would like to acknowledge the support provided for the present work by the Natural Sciences and Engineering Research Council of Canada (NSERC).

References

Akhlaque-E-Rasul, S. and Ganesan, R., 2009a. Buckling Response of Tapered Curved Composite Plates Based on Classical Shell Theories. *ICCM-17*, Edinburgh, UK.

Akhlaque-E-Rasul, S. and Ganesan, R., 2009b. The Compressive Response of Tapered Curved Composite Plates. *The Annual Technical Conference of American Society for Composites* (ASC), University of Delaware, Delaware, USA.

Akhlaque-E-Rasul, S. and Ganesan, R., 2009c. The Buckling Response of Tapered Curved Composite Plates-II. *The Annual Technical Conference of American Society for Composites* (ASC), University of Delaware, Delaware, USA.

Becker, M. L., 1979. Analytical/Experimental Investigation of the Instability of Composite Cylindrical Panels. *MSc Thesis*, Wright-Patterson AFB, Air Force Institute of Tech, OH, USA.

Bolotin. V. V., 2001. Mechanics of Delaminations in Laminate Composite Structures. Translated From *Mekhanika Kompozitnykh Materialov* 37(5/6), pp. 585-602.

Kant, T. and Swaminathan, K., 2000. Estimation of Transverse/Interlaminar Stresses in Laminated Composites-A Selective Review and Survey of Current Developments. *Composite Structures* 49, pp. 65-75.

Kee, Y. and Kim, J., 2004. Vibration Characteristics of Initially Twisted Rotating Shell Type Composite Blades. *Composite Structures* 64, pp. 151-159.

Piskunov, V. G. and Sipetov, V. S., October 1987. Calculation of Tapered Laminated Shells Consisting of Anisotropic Composite Materials for Static and Thermal Loads. Kiev Highway Institute, Translated from *Problemy Prochnosti* 10, pp. 79-82.

Salamon. N. J., 1980. An Assessment of the Interlaminar Stress Problem in Laminated Composites. *Journal of Composite Materials Supplement* 14, pp. 177.

Simitses, G. J., 1996. Buckling Of Moderately Thick Laminated Cylindrical Shells: A Review. *Composites Part B* 27b, pp. 581-587.

Soden, P.D., Kaddour, A.S. and Hinton, M.J., 2004. Recommendations for Designers and Researchers Resulting from the World-Wide Failure Exercise. *Composites Science And Technology* 64, pp. 589-604.

Tennyson, R. C., 1975. Buckling Of Laminated Composite Cylinders: A Review. *Composites* 6(17), pp. 17-24.

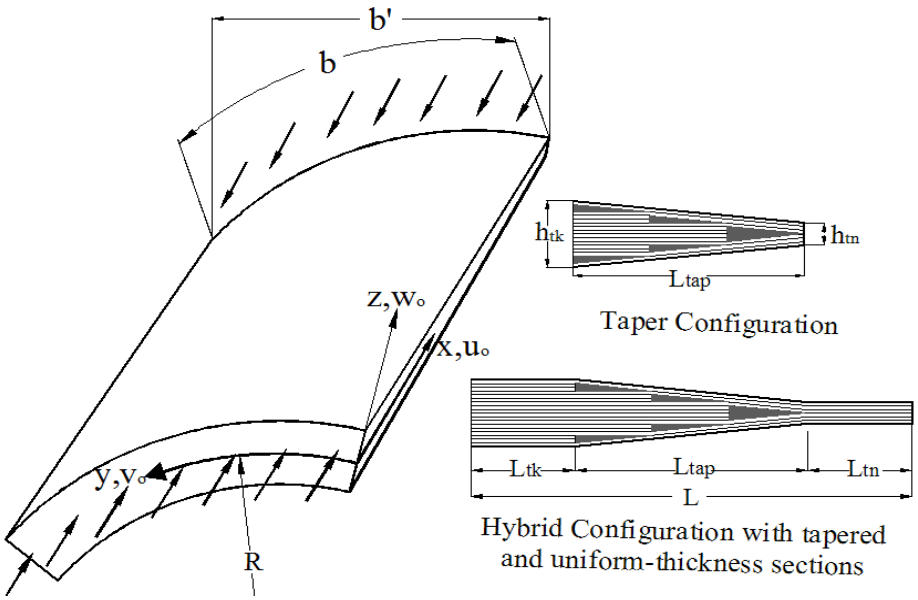

Figure 1: Different sections of curved laminated plate.

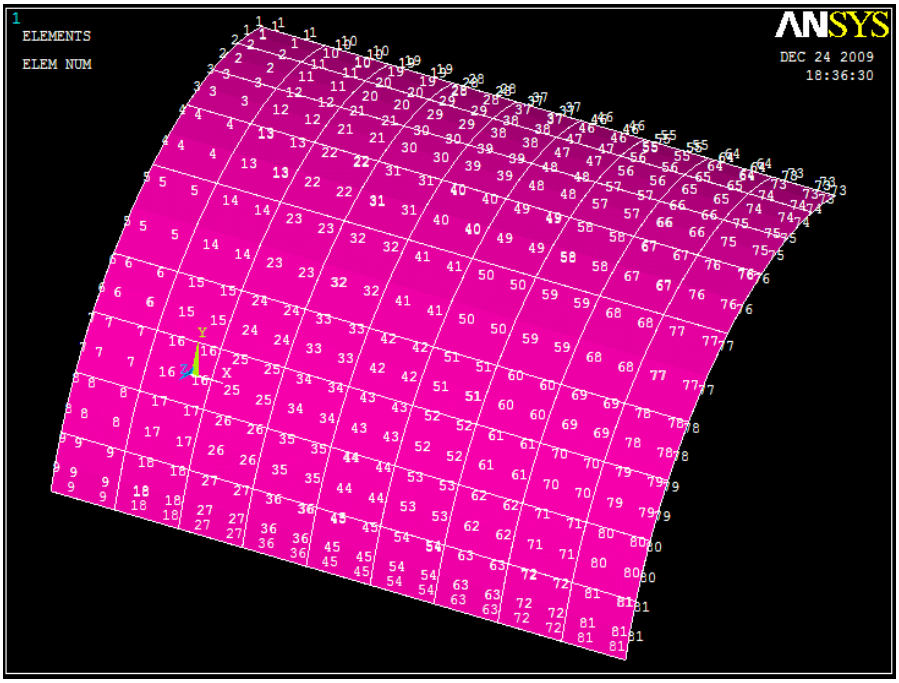

Figure 2: Finite element mesh for the cylindrical composite plate.

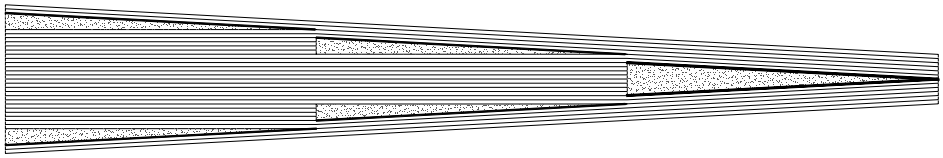

Figure 3: Longitudinal cross-section of the taper configuration with thin resin-rich layers.

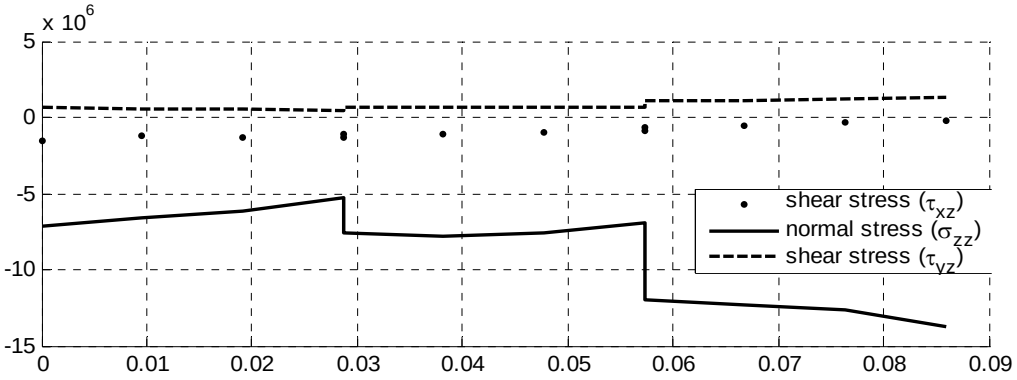

Figure 4: The stresses at the top 'resin-rich layers' with lay-up configuration LC_1 and the taper configuration for the taper angle of 1 degree.

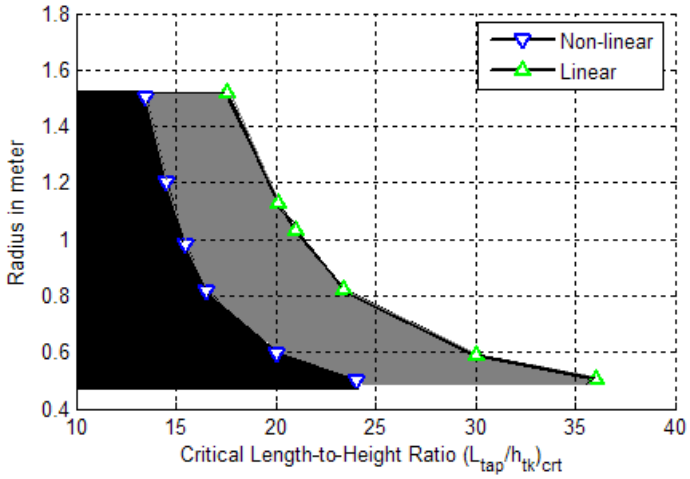

Figure 5: The effect of the radius of the tapered curved composite plate on the critical length-to-height ratio.

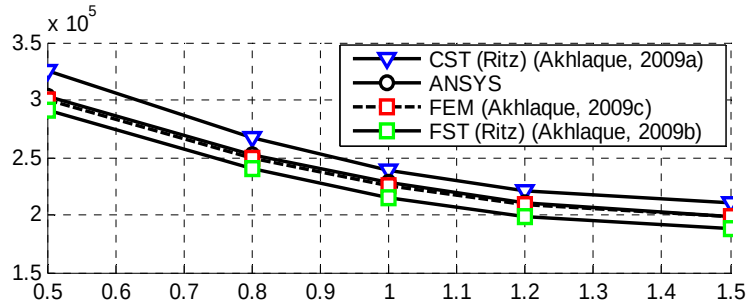

Figure 6: Variation of critical buckling load with the radius for the clamped hybrid laminate with LC_1 lay-up configuration.

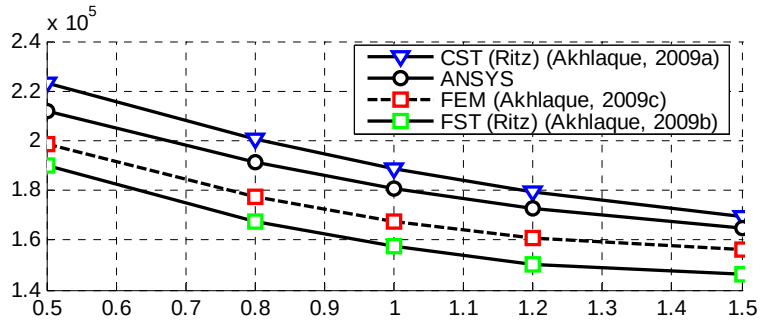

Figure 7: Variation of critical buckling load with the radius for the clamped hybrid laminate with LC_2 lay-up configuration.

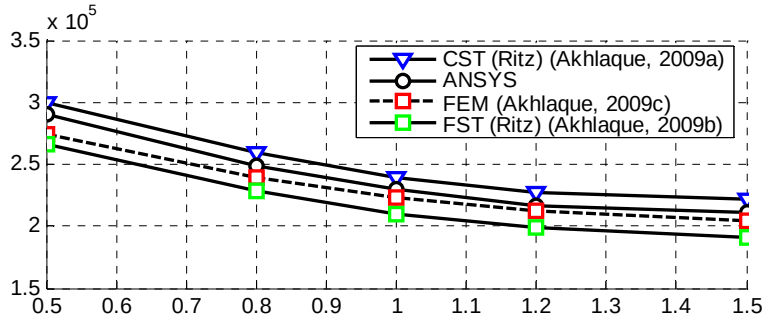

Figure 8: Variations of critical buckling load with the change of radius for the clamped hybrid laminate with LC_3 lay-up configuration.

Table 1: Material properties of NCT/301 graphite-epoxy composite ply material

Material Property	Value	Strength Property	Value
$E_{x''}$	113.9 GPa	X^t	1621 MPa
$E_{y''} = E_{z''}$	7.985 GPa	X^c	-1250 MPa
$G_{x''y''} = G_{x''z''}$	3.137 GPa	$Y^t = Z^t$	48.28 MPa
$G_{y''z''}$	2.852 GPa	$Y^c = Z^c$	-200 MPa
$\nu_{x''y''} = \nu_{x''z''}$	0.288	R_{yz}	25.00 MPa
$\nu_{y''z''}$	0.400	$S_{xz} = T_{xy}$	33.30 MPa

Table 2: Material properties of epoxy material used in NCT/301 ply

Material Property	Value	Strength Property	Value
$E_{x''} = E_{y''} = E_{z''}$	3.93 GPa	$X^t = Y^t = Z^t$	57.00 MPa
$G_{x''y''} = G_{x''z''} = G_{y''z''}$	1.034 GPa	$X^c = Y^c = Z^c$	-104 MPa
$\nu_{x''y''} = \nu_{x''z''} = \nu_{y''z''}$	0.37	$R_{yz} = S_{xz} = T_{xy}$	22 MPa

Table 3: Comparison of critical buckling load (N_{cr}) for uniform cylindrical plate using different methods

Lay-up Configuration	Becker (1979) $(N_{cr}L_{tap}^2)/(E_{x''}h_{tk}^3)$		CST (Akhlaque, 2009a) $(N_{cr}L_{tap}^2)/(E_{x''}h_{tk}^3)$	FST (Akhlaque, 2009b) $(N_{cr}L_{tap}^2)/(E_{x''}h_{tk}^3)$	Present $(N_{cr}L_{tap}^2)/(E_{x''}h_{tk}^3)$
	Theo.	Expt.			
$[90/0]_{2s}$	33.30	24.50	34.95	34.84	37.34

Table 4: List of lay-up configurations considered in the first ply failure analysis

Lay-up Configuration	Lengths of the Hybrid Configuration (m)				
	Thick Section	Thin Section	Thick Section	Tapered Section	Thin Section
LC_1	$[0/90]_{9s}$	$[0/90]_{3s}$	0.0382	0.1146	0.0382
LC_2	$[\pm 45]_{9s}$	$[\pm 45]_{3s}$	0.0382	0.1146	0.0382
LC_3	$[0_2/\pm 45_8]_s$	$[0_2/\pm 45_2]_s$	0.0382	0.1146	0.0382

Table 5: Critical buckling loads and first-ply failure loads of tapered curved laminates with lay-up configuration LC_1

Taper Angle in Degrees	Side Length of the Square Plate (m)	Buckling Load Using ANSYS® (x 10^4 N/m)	First-ply Failure Load Using ANSYS® (x 10^4 N/m)	Failure Location (FEN, FLN) [a]
0.10	0.8594	14.08	48.05	1, 2
0.50	0.1719	42.00	42.75	1, 2
0.75	0.1146	62.17	45.05	9, 3
1.00	0.0859	92.08	51.67	9, 3

[a] FEN and FLN denote, respectively, the failed element number and failed layer number at first-ply failure.

Table 6: Averaged maximum interlaminar shear stress of clamped-clamped tapered curved laminate with lay-up configuration LC_1

Taper Angle in Degrees	Side Length of Square Plate (m)	Compressive End Load (x 10^4 N/m)	Maximum Interlaminar Shear Stress, (MPa)	Location (EN, LLN) [b]	Remark
0.10	0.8594	48.05	1.01	63, 5	No Initiation of Delamination
0.50	0.1719	42.75	0.57	63, 5	
0.75	0.1146	62.17	0.99	55, 13	
1.00	0.0859	92.08	1.25	63, 5	

[b] EN and LLN denote, respectively, the element number and lower layer number adjacent to the interface where the interlaminer shear stress is maximum.